Nucleon density in the nuclear periphery determined with antiprotonic x rays: Calcium isotopes

F. J. Hartmann, R. Schmidt, B. Ketzer, and T. von Egidy
Physik-Department, Technische Universität München, D-85747 Garching, Germany

S. Wycech and R. Smolańczuk
Soltan Institute for Nuclear Studies, PL-00-681 Warsaw, Poland

T. Czosnyka, J. Jastrzębski, M. Kisieliński, P. Lubiński, P. Napiorkowski, L. Pieńkowski, and A. Trzcińska
Heavy Ion Laboratory, Warsaw University, PL-02-093 Warsaw, Poland

B. Kłos
Physics Department, Silesian University, PL-40-007 Katowice, Poland

K. Gulda and W. Kurcewicz
Institute of Experimental Physics, Warsaw University, PL-02-093 Warsaw, Poland

E. Widmann
CERN, CH-1211 Geneva 23, Switzerland
(Received 6 July 2001; published 13 December 2001)

X rays from the cascade of antiprotonic atoms have been studied by the PS209 Collaboration at LEAR of CERN. In this publication the strong interaction widths and shifts for calcium isotopes are presented. The isotopes ^{40}Ca,^{42}Ca,^{43}Ca,^{44}Ca, and ^{48}Ca have been investigated. The measured widths are compared with results from Hartree-Fock-Bogoliubov calculations. As a $CaCO_3$ target had been used for the measurement also the lowest antiprotonic transition of ^{16}O could be observed.

DOI: 10.1103/PhysRevC.65.014306 PACS number(s): 21.10.Gv, 36.10.−k, 25.43.+t

I. INTRODUCTION

Antiprotonic atoms provide important information on the antiproton-nucleus interaction and on the nuclear wave function, especially at the nuclear surface [1,2]. Consequently, the Warsaw-Munich collaboration PS209 at LEAR, CERN, Geneva, performed systematic measurements of antiprotonic x rays using targets of several isotope chains. Results on Yb isotopes were already published [3], a publication on Cd and Sn isotopes will follow [4], and several additional publications are in preparation. The collaboration also developed a new method to study the nuclear periphery by radiochemical analysis of residues after antiproton annihilation [5–8]. It is a special purpose of our studies to combine antiprotonic atom data with the radiochemical results in order to obtain consistent and precise information on the nuclear periphery [9].

The present publication deals with the magic Ca isotopes which deserve special interest since they include the doubly magic nuclei ^{40}Ca and ^{48}Ca. Hence the evolution of nuclear properties with the filling of the neutron shell may be observed. Previously antiprotonic x rays were measured for ^{40}Ca [10–12], but only data on the lowest antiprotonic-atom level were reported; these results will be discussed together with our measurements. ^{48}Ca was studied with the radiochemical method [8]. The antiproton-nucleus interaction was also determined by others using elastic scattering of antiprotons on ^{40}Ca [13,14].

After being slowed down in the target, the antiproton is captured by a target atom to form an antiprotonic atom. The initial orbit has a large principal quantum number n and the $\bar{p}$ cascades down towards levels with lower n under emission of Auger electrons and x rays. When the antiproton reaches a state around $n=4$ for light atoms such as calcium the strong interaction between the antiproton and the nucleus becomes sizeable and finally the antiproton annihilates. The strong antiproton-nucleus interaction results in shifts and widths of the lowest antiprotonic-atom transitions. If the shifts are larger than about 10 eV and the widths have the order of magnitude of the instrumental linewidth of the detectors (about 1 keV), they can be determined directly from the antiprotonic x-ray spectrum. In addition, it is possible to measure smaller strong-interaction widths which are roughly as large as the electromagnetic widths of the levels. For this method the intensity balance of transitions feeding and depopulating the level is used [15]. For Ca one may expect to measure the width of the level $(n,l)=(4,3)$ directly, as it has a value of several keV. However, since the transition $n=5 \rightarrow 4$ has a relative intensity of only 2%, its shape parameters could not be determined from the spectra of the individual isotopes. The *widths* of the levels $(n,l)=(6,5)$, on the other hand, are accessible via the intensity balance of the transitions feeding and depopulating the levels. The last transitions also allowed the determination of the $n=5$ level shift.

In the experiment to be described antiprotonic x rays from all stable calcium isotopes, except for ^{46}Ca, have been measured in order to obtain systematic information on the variation of the nuclear surface of the Ca isotopes. Details of the experiment and of the evaluation may be found in Ref. [16].

TABLE I. Target properties: thickness d, enrichment p, and number of antiprotons used.

Target	d(mg/cm^2)	p(%)	Number of $\bar{p}(10^8)$
^{40}Ca	52.4	99.9	6.0
^{42}Ca	55.3	76.3	4.7
^{43}Ca	56.3	31	2.4
^{44}Ca	60.7	89.6	5.9
^{48}Ca	46.9	97.27	7.3

II. EXPERIMENTAL ARRANGEMENT AND RESULTS

Our measurements were performed with the setup described already earlier [3,8]: Antiprotons from the beam of LEAR at CERN with an initial momentum of 106 MeV/c were registered with a telescope counter and stopped in the target. The antiprotonic x rays from the target were detected by three high-purity-Ge detectors. The properties of the targets are summarized in Table I. They consisted of pellets of $CaCO_3$ within mylar bags. Due to its small natural abundance a ^{46}Ca target was not available. The ^{43}Ca target had an enrichment of only 31(4)% [and contained 47(5)% of ^{40}Ca]. The on-line energy and efficiency calibration was performed in all cases with ^{152}Eu and ^{137}Cs sources.

Due to the low charge Z of the calcium nuclei the energies of the antiproton-atomic x rays are much smaller than those from the other antiprotonic atoms investigated by the PS209 Collaboration. As, due to the target thickness, the lowest energy which could be measured with the Ge detectors was limited to about 30 keV, only few transitions could be observed. This small number of transitions was sufficient to adjust the parameters for the cascade calculations, but the determination of the width of noncircular levels with the feeding transitions taken from cascade calculations [3] was not possible. Figure 1 shows typical antiprotonic x-ray spectra.

For the determination of the parameter α for the initial l distribution at $n=20$ of the calculated cascade

$$N(l) \propto (2l+1)\cdot \exp(\alpha \cdot l),$$

the intensities of the respective lines of all calcium isotopes were added (Table II). The best-fit result for α is 0.129(19), indicating an enhanced population of the high-l orbits at $n=20$ compared to that expected from a statistical distribution. Experimental and calculated x-ray intensities are in fair agreement, as shown in Fig. 2.

It is useful in another respect to sum up the spectra from the individual Ca isotopes. As may be seen from Fig. 1, upper part, the transition $n=5\rightarrow n=4$ is barely visible in the spectra from the individual calcium isotopes. In the sum of the collected spectra of all isotopes, however, this transition can be seen as a weak line (inset in Fig. 1, lower part). For the fit of this transition two Lorentzians convoluted with Gaussians were used. The resulting Lorentzian width gives the width due to the strong interaction. From the energy of the transition the energy shift from the purely electromagnetic transition energy was deduced. With its intensity the width of the level (5,4) was determined via the intensity balance. In Fig. 3 the results from the sum spectrum are presented together with the weighted mean values of the results from the upper transitions. These average values are interesting for a general comparison with calculations, as it

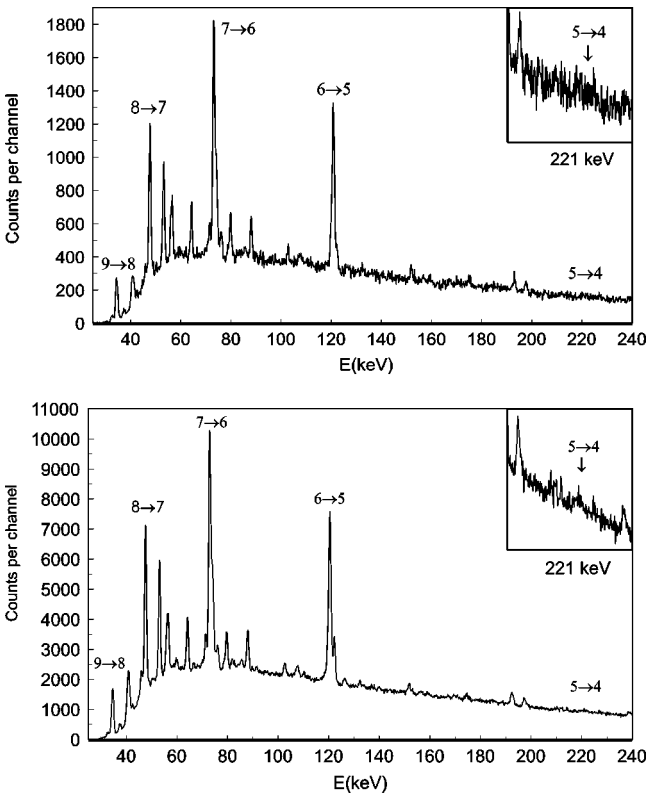

FIG. 1. Spectra of antiprotonic x rays from calcium. Upper part: spectrum from ^{48}Ca. Lower part: accumulated spectrum of all targets; the weights of the different calcium isotopes are for ^{40}Ca: 27%, ^{42}Ca: 18%, ^{43}Ca: 3%, ^{44}Ca: 24%, and for ^{48}Ca: 28% (determined from the number of antiprotons per isotope given in Table I).

TABLE II. Measured relative antiprotonic x-ray transition intensities normalized to the intensity of the line at 72 keV (mean values for all detectors and targets, see caption of Fig. 1).

Energy (keV)	Transitions		Relative intensity
120	6→5		85.0±4.3
72	7→6	11→8	100.0±5.0
47	8→7	14→10	75.1±3.8
32	9→8	12→10	66.2±3.4
23	10→9	13→11	38.0±2.1
192	7→5		8.9±0.6
119	8→6	11→7	16.0±0.9
79	9→7		14.1±0.8
55	10→8		13.2±0.7
239	8→5		3.4±0.6
151	9→6		5.5±0.5
102	10→7		5.7±0.4
174	10→6		2.7±0.7

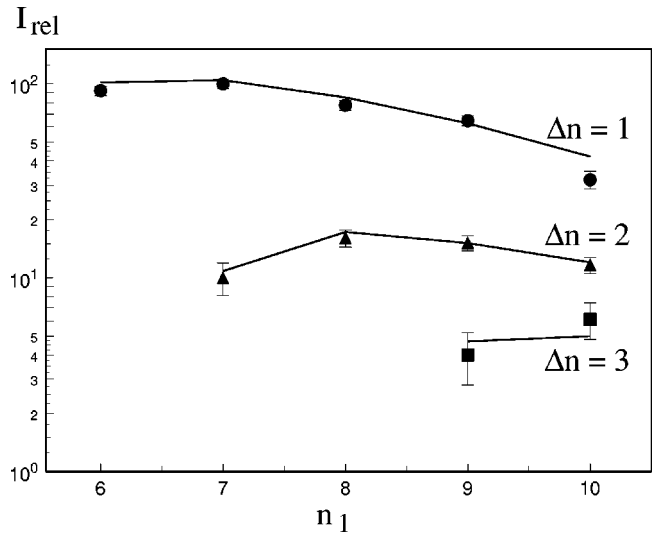

FIG. 2. Comparison of measured relative x-ray intensities with those calculated with the parameter $\alpha = 0.129$. The contribution of the different isotopes is given in the caption of Fig. 1. n_1 is the principal quantum number of the initial level. Only transitions weakly affected by strong interaction are shown.

has been performed, e.g., by Batty [17], but they will not be used in the following, because we are definitely looking for isotope effects.

From the measured intensity balance the strong-interaction widths Γ of the levels $(n,l)=(6,5)$ were determined according to Ref. [15]. Columns 2 and 3 of Table III show the radiative and Auger widths of this level. Small corrections for transitions parallel to the measured ones and for unobserved transitions from higher levels were taken from the optimized cascade calculation. The resulting strong-interaction widths are presented in Fig. 4 and Table III, column 4. From the measured energy of the transition $n=6 \rightarrow 5$ the strong-interaction energy shift ϵ has been deduced. This energy shift is the difference between the measured transition energies and those calculated with a purely electromagnetic potential [18]. The results are shown in Table III, last column, and plotted in Fig. 5.

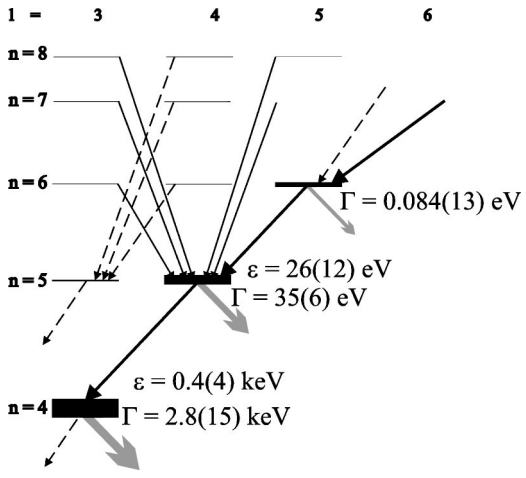

FIG. 3. Mean widths and shifts of all levels with measurable strong interaction effects. The weight of the different calcium isotopes is given in the caption of Fig. 1.

TABLE III. Calculated radiation width Γ_{em} and Auger width Γ_{Auger} for the levels (6,5) and mean width for the level (5,4) (weighted with the values given in the caption of Fig. 1); measured widths $\Gamma_S(6,5)$ for the level $(n,l)=(6,5)$ and energy shift $\varepsilon_{n=5}$ of the level $n=5$.

Target	Γ_{em} (eV)	Γ_{Auger} (eV)	$\Gamma_S(6,5)$ (eV)	$\varepsilon_{n=5}$ (eV)
^{40}Ca	0.669	0.007	0.059(18)	5(12)
^{42}Ca	0.650	0.007	0.080(28)	17(14)
^{43}Ca	0.641	0.007	0.073(42)	62(30)
^{44}Ca	0.633	0.007	0.077(23)	31(10)
^{48}Ca	0.604	0.006	0.116(17)	33(12)
(5,4)	1.639	0.003		

Since in the measurements carbonate targets were used, the x ray spectra contained also lines from antiprotonic oxygen and carbon. The transitions of antiprotonic carbon were hidden by other lines. The transition $n=5 \rightarrow n=4$ of ^{16}O (which contributes by 99.76% to the natural isotopic composition of oxygen) could be observed. As the oxygen isotopes had already been measured before [19], this was a good opportunity to test our method of evaluation. Additionally the uncertainty of the width and shift determined in Ref. [19] could be reduced by about 50%. The results, compared with the results of Ref. [19] are shown in Table IV.

III. DISCUSSION

Experimental and calculated widths of the level (6,5) in different Ca isotopes are compared in Table V. The width of the level (6,5) of ^{48}Ca is roughly twice as large as that of ^{40}Ca. This is due to the fact that the size of these nuclei increases with A. Such changes of the nuclear radii are also indicated by pion, alpha and proton scattering experiments, pionic atoms [2], and nuclear model calculations [20,21].

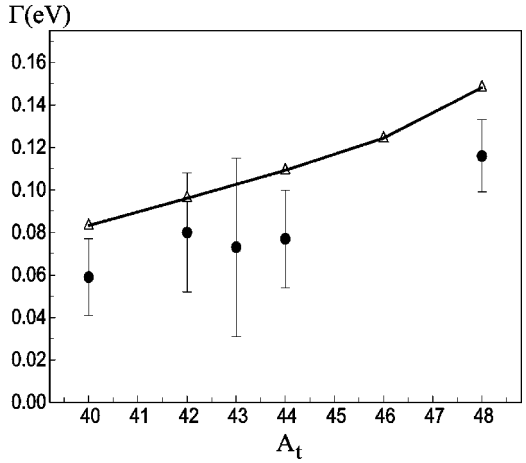

FIG. 4. Strong interaction widths of the level $(n,l)=(6,5)$ of $\bar{p}$-Ca derived via the intensity balance. The triangles show results from HFB-SkP nuclear-density calculations [28] with the effective length parameter $a=(-1.5-i2.5)$ fm.

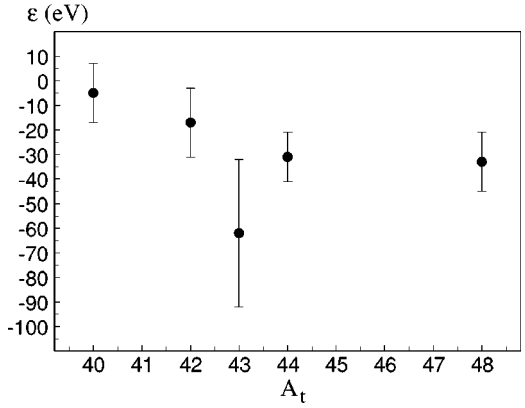

FIG. 5. Strong interaction shifts of $\bar{p}$-Ca: Differences $-\epsilon$ between the measured energies and the calculated purely electromagnetic energies of the transition $n=6\rightarrow 5$.

While for ^{40}Ca the level $n=5$ is not shifted, for ^{48}Ca it has a repulsive energy shift of (33 ± 12) eV. Due to the low enrichment of the ^{43}Ca target, there are large contributions of transitions of other calcium isotopes in the spectra from this target, which are superimposed on the ^{43}Ca lines. This fact results in large errors, which hide a possible effect of the unpaired neutron of ^{43}Ca.

Our experiments serve a double purpose: (1) to determine the $\bar{p}$-nucleus optical potential, and (2) to determine the neutron density distributions at the distant nuclear periphery and to relate them to similar findings in other experiments. In particular, the results obtained here are to be compared with the neutron halos found from nuclear reactions of the antiproton.

At this stage a detailed study of the optical potential in neutron-excess nuclei is not yet feasible. For such a purpose one needs more data and these are, fortunately, available or coming [4,22]. Some features are, however, clear already now. The standard optical potential

TABLE IV. Width and shift of the level $n=5$ of $\bar{p}^{16}$O.

	This experiment	Ref. [19]
Width	484(25) eV	495(45) eV
Shift	103(10) eV	112(20) eV

$$V^{\rm opt}(r)=\frac{2\pi}{\mu_{NN}}a\rho(r), \tag{1}$$

with $\rho(r)$ following the charge-density profiles, has been fixed by the studies of lower levels in light antiprotonic atoms. Such a potential works fairly well in the ^{40}Ca case but fails to reproduce the increasingly repulsive level shifts in heavier Ca isotopes. The attractive potential with $a\approx(-1.5-i2.5)$ fm [17] yields typical repulsive line shifts of about 3 eV in ^{40}Ca and similar values in other isotopes. It is apparent from Fig. 5 that these are the extra valence neutrons that act in an increasingly repulsive manner. This conclusion is supported by findings in other nuclei [22].

The neutron densities may be inferred from the absorptive level widths. These are to be calculated from the optical potential by

$$\Gamma/2=-\int|\Psi(r)|^2{\rm Im}[V^{\rm opt}(r)]d\vec{r}, \tag{2}$$

where Ψ is the atomic wave function which includes effects of nuclear interactions. In high-angular-momentum circular states one has $\Psi(r)\propto r^l\exp[(-Zr/B)n]$, where B is the Bohr radius. Thus Γ tests the high moments of the nuclear density distribution, and the dominant one is the $\langle r^{2l-2}\rangle$, i.e., $\langle r^8\rangle$ for the $(n,l)=(6,5)$ state of interest. A good estimate for the tested region is a layer of 2.5 fm thickness centered at about $r=c+1.5$ fm, with c the half-density radius. In this region

TABLE V. The $(n,l)=(6,5)$ level widths (in meV) for Ca isotopes, as calculated with $a=(-1.5-i2.5)$ fm and charge densities from several sources. The first two lines are calculated with the nuclear rms radii obtained from pion scattering data. Extreme values were assumed for the surface-thickness parameter t: $t=2.18$ fm (first line) and $t=2.47$ fm (second line). The last four lines are based on Fricke's charge densities [25] and extended neutron densities via Δc or Δt. The data in the last line were calculated with $a^*=(-1.1-i1.85)$ fm.

	^{40}Ca	^{42}Ca	^{43}Ca	^{44}Ca	^{48}Ca
Experiment	59(18)	80(28)	73(42)	77(23)	116(17)
Gibbs [23]	65	68		76	75
Gibbs [23]	90	97		108	110
de Vries *et al.* [24]	78				106
Fricke *et al.* [25]					
$\Delta c_{np}=0,\ \Delta t_{np}=0$	90	110	101	109	113
Δc_{np} optimized, $\Delta t_{np}=0$	90	107		119	139
$\Delta c_{np}=0,\ \Delta t_{np}$ optimized	90	112		134	188
$a^*=(-1.1-i1.85)$ fm, charge density from Ref. [25], Δt_{np} optimized	70	85	79	101	146

neither neutron nor proton (charge) densities are well known. We exemplify this problem by several calculations, given in Table V.

The electromagnetic measurements of charge densities (e.g., energy shifts of μ- and π-atomic levels and electron-scattering data) give very accurate values for the root-mean-square radius $R_{\rm rms}$. The surface diffuseness parameter t follows from electron scattering and its precision depends on the region of momentum transfers in the measurements. Knowing $R_{\rm rms}$, one may express it by

$$R_{\rm rms}^2 = 3/5c^2 + 7/5\pi^2[t/(4\ln 3)]^2, \tag{3}$$

through the parameters c and t of a two-parameter Fermi distribution

$$\rho(r) = \rho_0\{1+\exp[4\ln 3(r-c)/t]\}^{-1}, \tag{4}$$

but this relation does not allow us to determine c and t in a unique way. We illustrate this point in the second and third lines of Table V. Values for $R_{\rm rms}$ from pion scattering studies [23] are used with two arbitrary assumptions on the extreme values of t, $t=2.18$ fm and $t=2.47$ fm. These extremes cover the range of surface thickness parameters which are met in stable nuclei. The uncertainty in t is seen to generate a 30% uncertainty in $\Gamma(n=6,l=5)$. Fortunately there is agreement about the values of charge diffuseness in several of the Ca isotopes. The Γ based on electron-scattering results [24] are given in line 4 of Table V. These are fairly consistent with the results based on the compiled charge-density data of Fricke *et al.* [25], given in line 6 of the same table. The latter are described by a constant $t=2.30$ fm and $c=3.7721(13)$, 3.7690(15), 3.7843(13), and 3.7231(13) fm, respectively, for the four even Ca isotopes.

It is seen from these c values and from the widths that the charge densities in the first three Ca isotopes are almost the same. A small increase in the Γ values is essentially generated by changes in the atomic Bohr radii. One conclusion is that the much larger increase in the experimental widths and in particular the result for ^{48}Ca may not be attributed to an increasing charge density but stems from an increase of the neutron radius.

The differences $\Delta r_{np} = R_{\rm rms}^n - R_{\rm rms}^p$ between neutron and proton radii were derived from $\pi^{\pm}$, proton or α-particle scattering on nuclei. It is not easy to extract the bare-nucleon Δr_{np} from the profile of the optical potential used in the appropriate experimental analysis. However, to leading order in $t/(4\ln 3c)$ the changes $\Delta r_{np}^{\rm opt}$ and the changes Δr_{np} are equivalent. Consequently we implement these Δr_{np} values into the optical potential, Eq. (1), that consists now of two components ρ_p and ρ_n. Here the distribution ρ_n is to be understood as a folded density of bare neutrons with an annihilation form factor, in the same way as the charge density represents a bare-proton density folded with the proton electric form factor. The range of these form factors is assumed to be the same, 0.8 fm. The Δr_{np} are taken to be 0 (^{40}Ca), 0.04 fm (^{42}Ca), 0.08 fm (^{44}Ca), and 0.19 fm (^{48}Ca). The last three values are the averages of Δr_{np} values determined in several experiments presented in the review article by Batty *et al.* [2]. According to Eq. (3), these Δr_{np} values may be interpreted either as changes in the half-density radius or as changes in the diffuseness (or both). Let us study the consequences for the level widths. With the first choice one obtains a Δc_{np} which equals 0, 0.06, 0.12, 0.28 fm, respectively, for the four Ca isotopes, and the level widths are given in line 7 of Table V. One infers that the slope of $\Gamma(A)$ has not changed much. With the other choice, previously found in the analysis of our radiochemical data [22]—accommodation of the diffuseness values—one obtains $\Delta t_{np}=0$, 0.09, 0.18, and 0.44 fm, respectively. Now the slope of $\Gamma(A)$, given in line 8 of Table V follows roughly the experimental one. The results shown in this Table indicate that the effective length $a=(-1.5-i2.5)$ fm overestimates the widths. Of course agreement may be achieved by simply rescaling $\mathrm{Im}(a)$. Indeed in Ref. [26] a new value of $a^*=(-1.1-i1.85)$ fm was found. It was based on the old data in light nuclei and on the recent data in heavy nuclei [22]. The main change in the optical potential that lead to the rescaling is a removal of oscillator densities used previously in light nuclei. They have an incorrect asymptotic behavior. The densities of Fricke *et al.* [25] were used instead. The results obtained with the new value of a^* are given in Table V, last line.

As a^* is our best fit value, we use it to extract the neutron $R_{\rm rms}$ and Δr_{np} in ^{48}Ca. The number obtained is $\Delta r_{np} = 0.12^{-0.08}_{+0.04}$ fm and it should preferably be related to the change of the diffuseness $\Delta t_{np}=0.24$ fm. It may be compared to $R_{\rm rms}^p - R_{\rm rms}^n = 0.207(65)$ fm, or 0.166(101) fm, obtained from pionic atoms [27]. The two numbers quoted correspond to the different pionic optical potentials used in the fit. From pion-scattering experiments $R_{\rm rms}^p - R_{\rm rms}^n = 0.11(4)$ fm was obtained [23].

Now we present the data in a different way, instead, to make them almost independent from $V^{\rm opt}$. For high-l antiprotonic-atom states, Eq. (2) becomes approximately

$$\Gamma/2 = -\frac{2\pi}{\mu_{NN}}\mathrm{Im}(a)\int \Psi_{\rm Coul}(r)^2\rho(r)d\vec{r}, \tag{5}$$

where now $\Psi_{\rm Coul}(r)$ is the well-known Coulomb wave function. In the $(n,l)=(6,5)$ Ca states Eq. (5) is not perfect and one finds a moderate dependence of Γ on $\mathrm{Re}(a)$, in particular $\Gamma[\mathrm{Re}(a)=-1.5\ \mathrm{fm}]/\Gamma[\mathrm{Re}(a)=0]\approx 1.20$. On the other hand, minimum dependence of the ratios $\Gamma(^{48}\mathrm{Ca})/\Gamma(^{40}\mathrm{Ca})$, etc., on $\mathrm{Re}(a)$ as well as on $\mathrm{Im}(a)$ results. Within the range of likely values of a one finds this ratio to change as little as 1%. In this sense, the analysis of ratios is easier, as these are almost independent of $V^{\rm opt}$. The price to pay for such a simplification is the larger experimental error of the width ratio. The results are summarized in Table VI. The conclusions may be formulated in a similar way as above: (1) the charge densities are not adequate to reproduce the increase of the level widths with the atomic number and (2) the increase of $\Gamma(A)$ should be attributed rather to a change in the neutron diffuseness t than to one in c, in accordance with the findings from our radiochemical experiments [22].

TABLE VI. Ratios of $(n,l)=(6,5)$ widths in Ca isotopes. The potential for the lines 3 to 6 is based on $a=(-1.5-i2.5)$ fm, whereas the data in the last line were calculated with $a^*=(-1.1-i1.85)$ fm.

Experiment	$\frac{^{42}Ca}{^{40}Ca}$ 1.4(6)	$\frac{^{43}Ca}{^{40}Ca}$ 1.2(8)	$\frac{^{44}Ca}{^{40}Ca}$ 1.3(6)	$\frac{^{48}Ca}{^{40}Ca}$ 2.0(7)
Fricke *et al.* [25]				
$\Delta c_{np}=0,\ \Delta t_{np}=0$	1.11	1.12	1.20	1.25
Δc_{np} optimized, $\Delta t_{np}=0$	1.19		1.32	1.54
$\Delta c_{np}=0,\ \Delta t_{np}$ optimized	1.24		1.49	2.09
HFB calculations	1.19		1.34	1.58
$a^*=(-1.1-i1.85)$ fm, charge density from Ref. [25], Δt_{np} optimized	1.21		1.44	2.08

Our conclusion may be qualitatively understood with a simple shell model: the valence neutrons occupy the $f(7/2)$ shell and, due to the large angular momentum they possess, they tend to be localized in the surface region. The large-distance behavior is given by the asymptotic trend of the wave function $\phi_n \propto \exp(-\sqrt{2ME_B}r)(\hbar=c=1$ units). With a typical separation energy of 10 MeV one obtains $\phi_n^2 \propto \exp[-r/(0.73\ \text{fm})]$. This corresponds to a diffuseness parameter $t\approx 2.33$ fm, which is slightly larger than the diffuseness of protons obtained from the charge density. This rather simplistic view is supported to some extent by calculations with a Hartree-Fock-Bogoliubov model and Skyrme-III forces. These were done as described in Ref. [28]. The corresponding ratios, given in line 6 of Table VI, seem to be slightly short of the experimental ones, however.

The previous experiment on antiprotonic x rays from ^{40}Ca [11] produced fairly precise values of the (4,3) level shift and width. The numbers are given in Table VII with the corresponding calculations. These confirm the consistency with the value a^* for the scattering parameter. One also finds the average calculated (5,4) width of 28 eV to be consistent with the experimental one (see Fig. 3). As far as the shifts are concerned, the low (4,3) shift is reproduced quite well (see Table VII). On the contrary the calculated (5,4) shifts are in the range of 1 to 5 eV, i.e., much smaller than the experimental ones. This is in line with the related findings in Refs. [22,26]. The upper level shifts measured for small atomic-orbit nucleus overlap are difficult to understand.

TABLE VII. The shifts and widths of the $(n,l)=(4,3)$ level in ^{40}Ca [11]. The calculations are based on densities given by Fricke *et al.* [25].

Experiment	Γ(keV) 3.58(40)	ϵ(keV) 1.07(14)
Calculation $a=(-1.5-i2.5)$ fm	4.40	1.55
Calculation $a^*=(-1.1-i1.85)$ fm	4.10	1.11

Let us, finally, remark on the consistency of the x-ray experiment and the radiochemical measurement of the neutron-to-proton capture ratio in ^{48}Ca [8]. As already discussed, maximum absorption from the (6,5) orbit occurs roughly at $R_{1/2}+1.5$ fm. On the other hand, cold absorption of the antiproton, i.e., $\bar{p}$ absorption without subsequent reaction of the annihilation pions with the same nucleus, peaks at $R_{1/2}+2.5$ fm. With $\Delta r_{np}\approx 0.1$ fm from this experiment one finds the ρ_n/ρ_p ratios at these points to be 1.8 and 2.2, respectively. The experimental cold-absorption rate is $\Gamma^n_{\text{cold}}/\Gamma^p_{\text{cold}}=2.62(30)$ [8], which is consistent with the x-ray result.

To be more quantitative, we calculate the partial width Γ^p_{calc} for absorption on protons and next the ratio $\Gamma^n/\Gamma^p_{\text{calc}}=\Gamma_{\text{exp}}/\Gamma^p_{\text{calc}}-1$. This reflects the relative absorption rate in the atomic state. It becomes 1.58(38) and again should be compared to the respective ratio, 2.62(30), obtained from the radiochemical method. A word of caution is needed at this point. Consistency of the experiments has been achieved with the n/p annihilation ratio $R=\text{Im}(a_n)/\text{Im}(a_p)=1$. Much lower values are excluded by the ^{48}Ca data. The error bars for *both* experiments allow an R value in the region of 0.9 to 1.0. A better determination of R and a possible dependence of this ratio on the nucleon separation energies should be studied with the forthcoming data. It is clear that both experiments taken together put rather strong limits on this parameter.

IV. SUMMARY

Using the antiproton-atomic x-ray cascade for the calcium isotopes the antiproton-nucleus interactions were studied for very small antiproton-nucleus overlap. The shifts in the (5,4) levels and the widths of the (6,5) states were obtained. In addition, the (3,2) level in ^{16}O was remeasured and the older results were confirmed.

The widths of the (6,5) levels are consistent with the optical potential found recently in other measurements [26]. From these one may extract the neutron radius in ^{48}Ca which is consistent with other measurements. On the other hand we find the repulsive upper shifts of the (5,4) levels to be inconsistent with optical potentials fitted to widths and lower shifts in other atoms.

ACKNOWLEDGMENTS

We wish to thank the LEAR team for providing the intense, high-quality antiproton beam and Anna Stolarz of the Heavy Ion Laboratory in Warsaw and Katharina Nacke and Peter Maier-Komor of the Technical University Munich for the target preparation. Discussions with G. Fricke are appreciated. Financial support by the Accelerator Laboratory of the University and the Technical University of Munich as well as by the Polish State Committee for Scientific Research under Grant No. 2 P03B 048 15 is acknowledged. This work was also supported by the Volkswagen Foundation, Hannover, and by the Deutsche Forschungsgemeinschaft, Bonn.

[1] C.J. Batty, E. Friedman, and A. Gal, Phys. Rep. **287**, 385 (1997).
[2] C.J. Batty, E. Friedman, H.J. Gils, and H. Rebel, Adv. Nucl. Phys. **19**, 1 (1989).
[3] R. Schmidt, F.J. Hartmann, T. von Egidy, T. Czosnyka, J. Iwanicki, J. Jastrzębski, M. Kisieliński, P. Lubiński, P. Napiorkowski, L. Pieńkowski, A. Trzcińska, R. Smolańczuk, S. Wycech, B. Kłos, K. Gulda, W. Kurcewicz, and E. Widmann, Phys. Rev. C **58**, 3195 (1998).
[4] R. Schmidt, A. Trzcińska, T. Czosnyka, T. von Egidy, K. Gulda, F. J. Hartmann, J. Jastrzębski, B. Ketzer, M. Kisieliński, B. Kłos, W. Kurcewicz, P. Lubiński, P. Napiorkowski, L. Pieńkowski, and E. Widmann (unpublished).
[5] J. Jastrzębski, H. Daniel, T. von Egidy, A. Grabowska, Y.S. Kim, W. Kurcewicz, P. Lubiński, G. Riepe, W. Schmid, A. Stolarz, and S. Wycech, Nucl. Phys. **A558**, 405c (1993).
[6] P. Lubiński, J. Jastrzębski, A. Grochulska, A. Stolarz, A. Trzcińska, W. Kurcewicz, F.J. Hartmann, W. Schmid, T. von Egidy, J. Skalski, R. Smolańczuk, S. Wycech, D. Hilscher, D. Polster, and H. Rossner, Phys. Rev. Lett. **73**, 3199 (1994).
[7] P. Lubiński, J. Jastrzębski, A. Trzcińska, W. Kurcewicz, F.J. Hartmann, W. Schmid, T. von Egidy, R. Smolańczuk, and S. Wycech, Phys. Rev. C **57**, 2962 (1998).
[8] R. Schmidt, F.J. Hartmann, B. Ketzer, T. von Egidy, T. Czosnyka, J. Jastrzębski, M. Kisieliński, P. Lubiński, P. Napiorkowski, L. Pieńkowski, A. Trzcińska, B. Kłos, R. Smolańczuk, S. Wycech, K. Gulda, W. Kurcewicz, and E. Widmann, Phys. Rev. C **60**, 054309 (1999).
[9] A. Trzcińska, J. Jastrzębski, P. Lubiński, F.J. Hartmann, R. Schmidt, T. von Egidy, and B. Kłos, Phys. Rev. Lett. **87**, 082501 (2001).
[10] H. Poth in *Lecture Notes in Physics*, edited by H. Arachi *et al.* (Springer, Berlin, 1985), p. 357.
[11] H. Poth, Workshop on Antimatter Physics at Low Energies, Batavia, IL, Report No. Cern-EP/86-105, 1986.
[12] H. Poth, Nucl. Phys. **A478**, 655c (1988).
[13] D. Garreta, P. Birien, G. Bruge, A. Chaumeaux, D.M. Drake, S. Janouin, D. Legrand, M.C. Lemaire, B. Mayer, J. Pain, J.C. Peng, M. Berrada, J.P. Bouquet, E. Monnand, P. Perrin, E. Aslanides, O. Bing, J. Lichtenstadt, and A.I. Yavin, Phys. Lett. **149B**, 64 (1984).
[14] S. Janouin, M.C. Lemaire, D. Garreta, P. Birien, G. Bruge, D.M. Drake, D. Legrand, B. Mayer, J. Pain, J.C. Peng, M. Berrada, J.P. Bouquet, E. Monnand, J. Mougey, P. Perrin, E. Aslanides, O. Bing, J. Lichtenstadt, and A.I. Yavin, Nucl. Phys. **A451**, 541 (1986).
[15] H. Koch, G. Poelz, H. Schmitt, L. Tauscher, G. Backenstoss, S. Charalambus, and H. Daniel, Phys. Lett. **28B**, 279 (1968).
[16] R. Schmidt, Ph.D. thesis, Technische Universität München, Herbert Utz Verlag, Munich, 1999.
[17] C.J. Batty, Nucl. Phys. **A372**, 433 (1981).
[18] E. Borie, Phys. Rev. A **28**, 555 (1983).
[19] Th. Köhler, P. Blüm, G. Büche, A.D. Hancock, H. Koch, A. Kreissl, H. Poth, U. Raich, D. Rohmann, G. Backenstoss, Ch. Findeisen, J. Repond, L. Tauscher, A. Nilsson, S. Carius, M. Suffert, S. Charalambus, M. Chardalas, S. Dedoussis, H. Daniel, T. von Egidy, F.J. Hartmann, W. Kanert, G. Schmidt, J.J. Reidy, M. Nicholas, and A. Wolf, Phys. Lett. B **176**, 327 (1986).
[20] A. Brown, E. Massen, and P.E. Hodgson, J. Phys. G **5**, 1655 (1979).
[21] P.E. Hodgson, Contemp. Phys. **22**, 511 (1981).
[22] A. Trzcińska, J. Jastrzębski, T. Czosnyka, T. von Egidy, K. Gulda, F. J. Hartmann, J. Iwanicki, B. Ketzer, M. Kisieliński, B. Kłos, W. Kurcewicz, P. Lubiński, P. Napiorkowski, L. Pieńkowski, R. Schmidt, and E. Widmann, Nucl. Phys. **A692**, 176c (2001).
[23] W.R. Gibbs and J.-P. Dedonder, Phys. Rev. C **46**, 1825 (1992).
[24] H. de Vries, C.W. de Jager, and C. de Vries, At. Data Nucl. Data Tables **36**, 495 (1987).
[25] G. Fricke, C. Bernhardt, H. Heilig, L.A. Schaller, L. Schellenberg, E.B. Shera, and C.W. de Jager At. Data Nucl. Data Tables **60**, 177 (1995).
[26] S. Wycech, Nucl. Phys. **A692**, 29c (2001).
[27] R.J. Powers, K.C. Wang, M.V. Hoehn, E.B. Shera, H.D. Wohlfahrt, and R. Kunselman, Nucl. Phys. **A336**, 475 (1980).
[28] S. Wycech, J. Skalski, R. Smolańczuk, J. Dobaczewski, and J.R. Rook, Phys. Rev. C **54**, 1832 (1996).